

The precious set of radio-optical reference frame objects in the light of Gaia DR2 data

Valeri V. Makarov, Ciprian T. Berghea, Julien Frouard, Alan Fey

*United States Naval Observatory, 3450 Massachusetts Ave. NW, Washington, DC
20392-5420, USA*

Henrique R. Schmitt

Naval Research Laboratory, 4555 Overlook Ave. SW, Washington, DC 20375, USA

valeri.makarov@navy.mil

ABSTRACT

We investigate a sample of 3413 *International Celestial Reference Frame* (ICRF3) extragalactic radio-loud sources with accurate positions determined by VLBI in the S/X band, mostly active galactic nuclei (AGN) and quasars, which are cross-matched with optical sources in the second Gaia data release (Gaia DR2). The main goal of this study is to determine a core sample of astrometric objects that define the mutual orientation of the two fundamental reference frames, the Gaia (optical) and the ICRF3 (radio) frames. The distribution of normalized offsets between the VLBI sources and their optical counterparts is non-Rayleigh, with a deficit around the modal value and a tail extending beyond the 3σ confidence level. A few filters are applied to the sample in order to discard double cross-matches, confusion sources, and Gaia astrometric solutions of doubtful quality. *Panoramic Survey Telescope and Rapid Response System* (Pan-STARRS) and *Dark Energy Survey* (DES) stacked multicolor images are used to further deselect objects that are less suitable for precision astrometry, such as extended galaxies, double and multiple sources, and obvious misidentifications. After this cleaning, 2643 quasars remain, of which 20% still have normalized offset magnitudes exceeding 3, or a 99% confidence level. We publish a list of 2119 radio-loud quasars of prime astrometric quality. The observed dependence of binned median offset on redshift shows the expected decline at small redshifts, but also an unexpected rise at $z \sim 1.6$, which may be attributed to the emergence of the C IV emission line in the Gaia's *G* band. The Gaia DR2 parallax zero-point is found to be color-dependent, suggesting an uncorrected instrumental calibration effect.

Subject headings: astrometry — reference systems — quasars: general — galaxies: nuclei

1. Introduction

The second release of the Gaia mission data (Gaia DR2, Prusti et al. 2016; Brown and Gaia Collaborators 2018) made huge strides both in astrometric accuracy and in the number of measured objects compared with the first release in 2016. As explained in Lindegren et al. (2018), the reference system of the Gaia DR2 astrometric solution, which defines the orientation of the coordinate triad in space and the rigid spin of the entire ensemble of 1.7 billion objects, is not independent. The coordinates of Gaia sources were adjusted to the International Celestial Reference Frame (ICRF) using a preliminary solution for the version 3. The proper motions were also adjusted through a 3D rotation using a much greater sample of mid-infrared identified quasars and AGNs from the MIRAGN catalog (Secrest et al. 2015). In the latter case, the constraint is derived from the prior information that quasars should have vanishingly small proper motions due to their large distances from the observer, except for the small effect of *secular aberration* (e.g., Kopeikin & Makarov 2006). The former tie, on the other hand, requires a much more restricted sample of special objects, which we call Radio-Optical Reference Frame (RORF) objects. These should be radio-loud, unresolved AGNs of supreme astrometric quality, amenable to VLBI position measurements at the microarcsecond level. At the same time, RORF objects must have sufficiently optically bright counterparts to be observed by Gaia.

Radio-loud quasars and AGNs are not ideal objects for optical astrometry (Makarov et al. 2012). The nearby AGNs are often associated with their elliptical or spiral host galaxies. The extended substrate image perturbs Gaia astrometry at the centroid fitting level, as the latter procedure was designed for unresolved, point-like sources in Gaia DR1 and DR2 (Fabricius et al. 2016). According to the “fundamental plane” relation proposed by Hamilton et al. (2008), the magnitude difference in V between the host galaxy and the nucleus is larger for luminous nuclei. The statistical equality is achieved at $M_V(\text{nuc}) = -22.8$, but already at $M_V(\text{nuc}) = -25.7$, the host galaxy is typically 2 mag fainter than the nucleus. This result was based on observations of 70 AGNs with $0.06 \leq z \leq 0.46$. Most of the radio-loud AGNs investigated here have $z > 0.5$ and very luminous nuclei, so the host galaxy perturbation should be much diminished for the bulk of the sample. We also apply additional vetting (Section 3.1) based on high-quality composite images from *Panoramic Survey Telescope and Rapid Response System* (Pan-STARRS) and *Dark Energy Survey* (DES) to remove AGNs projected against conspicuous galaxies. This also helps to get rid of close

double and multiple sources, possible lenses, and confusion sources.

The existence of large differences in the radio-optical positions of reference AGNs of ~ 10 mas was suspected by Zacharias & Zacharias (2014), but the relatively modest accuracy of the dedicated ground-based CCD observations with the 0.9 m telescope could not provide a confident detection. Up until the advent of Gaia data, the bulk of optical counterparts of RORF objects were considered to provide high-quality absolute reference. Berghea et al. (2016) used the VLBI-measured radio positions from the Optical Characteristics of Astrometric Radio Sources (OCARS) compilation (Malkin 2013; Titov & Malkin 2009; Malkin 2016) as hard constraints for a global astrometric adjustment of the Pan-STARRS catalog and investigated the deviant cases in the process. They determined that a non-negligible fraction of the VLBI sources ($\sim 10\%$) have mismatching optical positions in Pan-STARRS beyond the statistical expectation. A list of sources was published that should not be used as RORF objects because they exhibit obvious signs of perturbations on the high-resolution Pan-STARRS maps. The relatively low level of astrometric precision in Pan-STARRS (50–70 mas per coordinate) did not allow the authors to study the bulk of cases apart from the gross discrepancies.

The two data releases of Gaia allowed us to look at the problem through the magnifying glass of space-grade astrometry. Based on much more accurate DR1 data, Petrov & Kovalev (2017) concluded that 6% of sources with accurate VLBI positions have significant differences at 99% confidence level, while Makarov et al. (2017) estimated that more than 4% of the smaller ICRF2 sample (Fey et al. 2015) differ in their radio and optical positions by more than 12σ , after removing as many contaminants as possible.

In this paper, we review the problem of radio-optical offsets in the light of Gaia DR2 data. Our goal is not to validate the results of the DR2, as was done by ?. We compute and analyze the absolute and relative position differences “Gaia – VLBI” in Section 2 and confirm that these differences are even more common and pronounced than what the previous studies have revealed. After a few types of cleaning and filtering are applied (Section 3.1), the final selection of best quality RORF objects is discussed and presented in Section 3.2. We investigate a possible relation to the deviation of Gaia parallaxes from the expected zero in Section 4. Possible correlation of radio-optical offsets with redshift is addressed in Section 5, and conclusions are drawn in Section 6.

2. Radio-optical offsets

We selected all Gaia DR2 objects within $1''$ of each ICRF3¹ source, using the VLBI positions listed in ICRF3. The search radius corresponds to the upper limit of genuine positional differences found in the previous analysis (Makarov et al. 2017). This search resulted in 3413 tentative matches, with some of the radio sources associated with more than one Gaia source. After cross-matching this list with the OCARS compilation² (August 2018 version), we discard all objects labeled as galaxies (G) and BL Lacertae-type (BL), which are known to be problematic sources for optical astrometry because of the host galaxy contribution in their images. After also cleaning of obvious misses and confusion sources, 3020 tentative matches remain. Following the steps of the previous study based on Gaia DR1 (Makarov et al. 2017), we compute the following quantities for each match: d_1 and d_2 are the tangential angular coordinate differences in the sense Gaia – VLBI in right ascension (times cosine declination) and declination, respectively; u is the normalized total offset

$$u = \Delta/\sigma_\Delta = \sqrt{d_1^2 + d_2^2}/\sigma_\Delta. \quad (1)$$

In the calculation of the formal standard deviation of the absolute offset, σ_Δ , the complete 2×2 block of the covariance matrix was used, as described in Mignard et al. (2016) and Makarov et al. (2017). This method fully takes into account the covariances of coordinate uncertainties in both VLBI and Gaia measurements. The histogram of normalized offsets in Fig. 1 peaks approximately at the maximum probability density of the expected (for a normal distribution of coordinate uncertainties) Rayleigh distribution with a scaling parameter of 1. A small shift of the histogram peak to higher values of u is probably caused by the formal errors of Gaia, which are known to be underestimated (Lindegren et al. 2018). The most conspicuous feature is a deficit of values around the mode, which is caused by a long and shallow tail stretching to large offsets. The coordinate differences are definitely not Gaussian, and a significant fraction of offsets is much greater than what the estimated astrometric precision suggests. A similar behavior, albeit at a much coarser precision, was seen for the Gaia DR1 positions.

¹The S/X ICRF3 catalog is available for download at <http://hpiers.obspm.fr/webiers/newwww/icrf/>.

²http://www.gaoran.ru/english/as/ac_vlbi/ocars.txt.

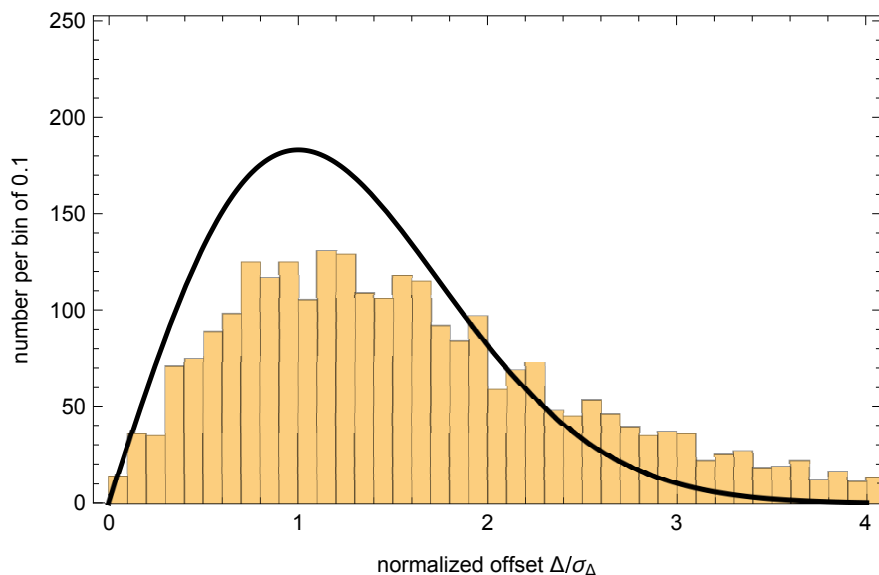


Fig. 1.— Histogram of normalized Gaia–VLBI offsets u (Eq. 1) for a sample of 3020 astrometric quality RORF objects, after preliminary cleaning and filtering procedures have been applied. The graph is limited to $u < 4$ mas but the sample distribution extends to above 4000. The black curve shows the scaled Rayleigh distribution with a scaling parameter $\sigma = 1$, which is expected to fit the sample distribution if the coordinate errors are Gaussian-distributed with the given formal errors.

3. Toward a clean set of RORF sources

3.1. Independent vetting

As our second step toward a clean sample of RORF objects, we investigated some of the astrometric and photometric criteria suggested in the literature, aimed at removing perturbed and low-quality solutions in Gaia DR2. A large number of Gaia DR2 astrometric solutions is perturbed by various factors, including calibration issues, double sources, and crowding contamination. These solutions may not be reliable, in which case they should not be used for this analysis. The filter described by Arenou et al. (2018, their Eq. 1) uses the reduced χ^2 statistic of the residuals and sets up a magnitude-dependent threshold on the excess scatter. Applying this filter to our sample of 3020 cross-matched Gaia-OCARS sources removes 249 of them, i.e., 8%. To estimate the effectiveness of this filter, we compare the distributions of the normalized offsets u for the sets of discarded sources and the 2771 objects that passed the (χ^2_{astro}) filter. Fig. 2 shows the results of this comparison represented as a “Q-Q plot”, where quantiles of the empirical distribution of u values of the vetted sources (ordinate) are mapped against the same quantiles for the 2771 accepted objects (abscissa). The straight line of unit slope shows where the quantile sequence should lie in case the two independent distributions are identical. The quantile values systematically lie above this line. This means that the discarded objects have systematically larger values of u at any quantile than the accepted objects. Thus, we find this quality criterion efficient for cleaning the sample of RORF objects.

The other major quality filter suggested in the literature is that of photometric nature (Eq. 2 in Arenou et al. 2018), which is aimed at detecting solutions with a significant impact of extraneous signal using the excess color factor. This filter would remove a hefty 1270 objects, or 46% of the sample. Analysis of the position offsets revealed that the filter was not efficient in reducing the scatter or removing extreme outliers. A Q-Q plot similar to Fig. 2, not reproduced here for brevity, shows that quantile values for sources with a G -band excess, referenced to their counterparts for sources without this excess, lie close to the line of unit slope, or even below it. Removing objects with the photometric excess would not make the distribution of offsets tighter. The inefficiency of this criterion may be related to the fact that quasars have spectral energy distributions significantly different from field stars. We decided to not apply this filter to our sample of radio-loud quasars, but to clean it further using other methods independent of the Gaia data.

We further find that four ICRF3 sources are each cross-matched to two different Gaia DR2 entries. This is not surprising, because the angular resolution of Gaia measurements is better than $1''$, which is our search radius. The optical counterparts may be optical pairs

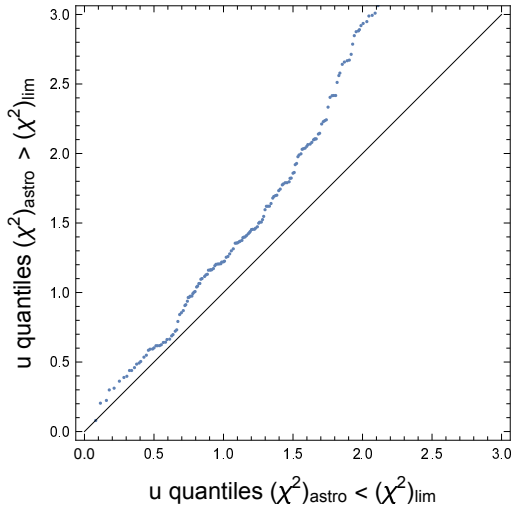


Fig. 2.— Quantile plots of normalized residuals u for RORF sources with high values of reduced χ^2 statistics on astrometric residuals in Gaia DR2 against the quantiles for sources passing this filter. The straight line represents the locus of quantile values when the two distributions are identical.

or genuine double AGNs. To avoid possible astrometric errors caused by closely separated images, we remove all eight cross-matched counterparts from the list.

Following the method first proposed in Makarov et al. (2017), we collected a large number of high-quality images of RORF objects and visually inspected all of them. Some of the radio-loud AGNs in our sample reside in the cores of luminous galaxies. Astrometric solutions for extended objects are perturbed, which possibly explains why the frequency of outliers is higher at small redshifts (Fig. 6). OCARS provides specific morphological classification of the optical counterpart, which we already used to remove all objects flagged as “galaxies”. The major source of images came from the collection of colored stacked (Pan-STARRS) available through the Mikulski Archive for Space Telescopes (MAST) provided by the STScI. Pan-STARRS includes a multipassband panoramic survey of the northern 3/4 of the sky (above $\text{Dec} \simeq -30^\circ$, Chambers et al. 2016) so only three quarters of the sample can be reviewed this way. For the southern sky, we used the recently published access facility to stacked (DES) images (Morganson et al. 2018). The quality of both Pan-STARRS and DES images is superior to the previous surveys, routinely reaching better than $1''$ resolution.

We performed a blind inspection of collected images without referencing the position offsets. The images were separated into four groups, based on the visual inspection. One group was comprised of objects where the presence of a host galaxy was obvious to the eye. Tightly spaced double or multiple sources were separated into another group. We also found

a smaller number of objects where no optical counterpart was visible at the VLBI location, but a faint optical source (likely, a chance field star) was present at separations $s \gtrsim 0''.5$. Finally, the largest group included sources that did not reveal any obvious problems and looked point-like. Fig. 3 shows a few examples of DES images, which indicate problematic cases for optical astrometry. Any deviation from a nominal star-like image can significantly perturb the Gaia-determined photocenter, because a single template line spread function was applied for each CCD and each gate (Fabricius et al. 2016) in the low-level pipeline processing. These perturbations are not always captured by the χ^2 -based residual statistic, apparently.

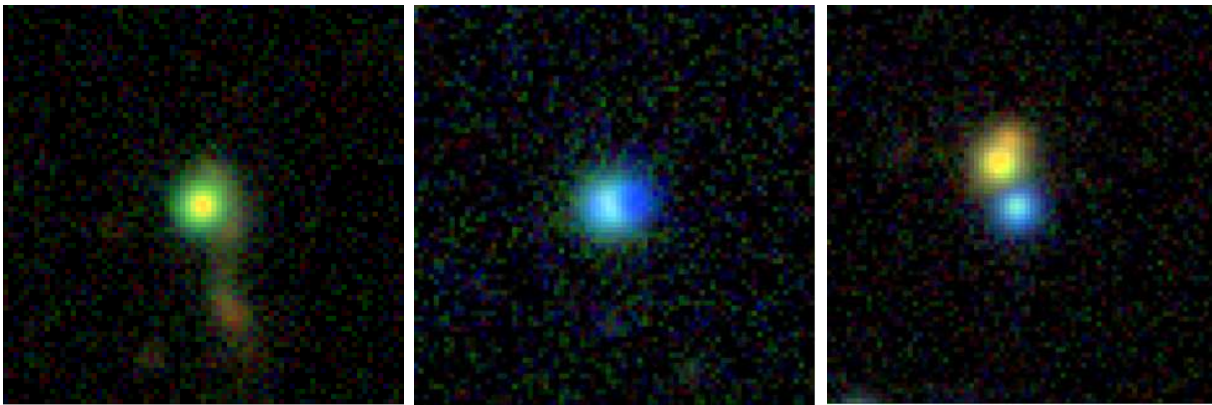


Fig. 3.— DES images of three representative types of optical counterparts of VLBI-measured radio-loud AGN, which are deemed not suitable for a RORF tie. Each image is $20''$ on a side, with north up and east to the left. The matched radio source is exactly at the center of each image. Left: PKS 0521 – 403, an interacting galaxy. Middle: IVS B0307 – 362, possibly double or microlensed. Right: IVS B2203 – 617, a close multiple object.

To estimate the effectiveness of the blind image vetting, we compare the distributions of the normalized offsets u for the sets of extended sources and double or multiple sources using the empirical distribution of star-like sources as reference. The corresponding Q-Q plots indicate that the vetting of remaining extended optical images is moderately successful, as the quantile values for them are systematically higher than the quantiles for point-like sources. On the other hand, the vetting of resolved double sources is not efficient, removing only several extreme outliers at $u > 4$. It appears that double images at separations greater than $1''$ do not much perturb Gaia astrometric solutions. However, we decided to remove all identified double, extended, and misplaced images from the sample in view of their relatively small number. It should be noted that for ICRF3 sources in some areas south of $\text{Dec} = -30^\circ$ without DES coverage, no images of comparable quality are available.

3.2. The precious set

The final “clean” sample counts 2643 RORF objects. Thus, the cleaning removed 23% of the starting selection. The histogram of normalized offsets u in Fig. 1 is still quite far from the expected Rayleigh(1) distribution. The pronounced deficit of values in the core is caused by the excess of statistically large position offsets. This result can be expressed in terms of the statistical survival function, which estimates that 99% of a Rayleigh-distributed sample should have values less than 3. In fact, 20% of the cleaned sample (524 sources) have normalized position differences in excess of 3. The rate of statistically significant offsets is dramatically larger than the previous estimate based on Gaia DR1. The reason for this is probably the much improved accuracy of Gaia DR2 positions compared with DR1. We can more clearly see now that the bulk of radio-loud quasars have their optical photocenters displaced at the submilliarcsecond level.

Still, these objects straddling the radio and optical domains, provide the best chance to establish an accurate reference frame tie between Gaia and VLBI, as far as accurate positions are concerned. We therefore suggest an additional empirical cut of the sample at $u = 3$ to generate the cleanest set of RORF objects, which pass all the currently available quality criteria. This “precious set” of 2119 sources is published in its entirety online. Table 1 provides a small cutout of the file. VLBI coordinates from ICRF3 (columns 2 – 3) and redshifts (column 10) are combined with astrometric and photometric information from Gaia DR2 (columns 4 – 9) followed by position differences (columns 11 – 13) derived in this paper.

4. The parallax zero-point

Quasars can be considered zero-parallax objects because of the great distances separating them from the Sun. The parallaxes of the radio-loud sources from OCARS measured by Gaia provide a method to estimate the so-called zero-point error, which is a constant bias applied to all objects. Based on a much larger selection of optically identified quasars from Secrest et al. (2015), Lindegren et al. (2018) estimated the global zero-point at $-29 \mu\text{as}$. Individual parallax determination can be affected by blended confusion sources and extended structures of the host galaxies. Here we use our clean sample (before the $u < 3$ cut) to estimate the parallax zero-point for 2465 radio-loud sources.

The histogram of measured parallaxes in Fig. 4 has a complex non-Gaussian shape because it is composed of objects from a range of magnitudes, whose intrinsic astrometric precision also varies over a wide range. The core of the distribution is sharp, and it is

Table 1. Best quality radio-optical reference frame objects

(1) [†]	(2)	(3)	(4)	(5)	(6)	(7)	(8)	(9)	(10)	(11)	(12)	(13)
0948 + 658	148.134135797	65.6336714927	1066310912103182464	0.110	0.145	18.034	18.295	17.526	nan	-0.827	0.892	0.763
1016 + 635	154.961986900	63.3337852583	1052151882396770944	-0.041	0.161	18.462	18.568	17.590	2.025	-0.073	-0.017	0.299
0839 + 687	130.954589771	68.5547652916	1118095435870099584	-0.539	0.625	20.010	20.089	19.571	nan	-0.278	0.969	1.806
0859 + 681	135.971479324	67.9563015749	1117118691587459200	-0.175	0.195	18.313	18.613	17.722	1.499	0.120	0.194	1.09
0928 + 653	143.227406594	65.1281379721	1067919119657621504	nan	nan	20.996	21.107	19.888	nan	-0.915	0.060	0.770
0810 + 646	123.663293069	64.5227850264	1091852056117623936	-0.037	0.046	15.869	16.269	15.173	0.239	-0.181	-0.028	0.547
0759 + 641	120.967330777	64.0539924397	1091417229331516032	0.027	0.304	18.889	19.046	18.398	nan	-0.014	0.450	1.592

[†]Columns:

(1) IERS designation; (2) ICRF3 right ascension, deg; (3) ICRF3 declination, deg; (4) Gaia unique source identifier; (5) Gaia parallax, mas; (6) Gaia parallax error, mas; (7) G magnitude; (8) BP magnitude; (9) RP magnitude; (10) redshift z from OCARS; (11) RA difference (times $\cos \delta$) “Gaia–ICRF3”, mas; (12) Dec difference “Gaia–ICRF3”, mas; (13) normalized position difference u .

obviously shifted to the negative side. We used two kinds of robust statistics to estimate the “average” shift. The median of all parallaxes is equal to $-35 \mu\text{as}$, and the biweight location³ (with a scaling parameter of 6) is also $-35 \mu\text{as}$. The closeness of these estimates indicates a stable result, but they are somewhat larger in magnitude than the previous (Lindgren et al. 2018) estimate $-29 \mu\text{as}$. Although the zero-point error is expected to originate from a specific time-dependence of the Gaia basic angle, which is hard to calibrate with the desired accuracy, the color-dependent calibration term may interfere with this parameter too. The large collection of MIRAGN objects, selected by their midinfrared colors, may have different optical colors from the radio-loud VLBI AGNs. The latter group shows a large degree of variability in magnitudes and colors, and a complicated dependence of “quiescent” magnitudes with redshift z (Berghea et al., in preparation). There seem to be two subpopulations of ICRF3 sources segregated in the color-redshift plane, with the nearby objects (small z) being typically redder and less variable than the more distant ones. This segregation also shows in Fig. 5, right panel, where we used the nominal BP–RP colors from Gaia DR2 and the redshifts of 2051 objects to estimate how the median color depends on redshift. We detect a sharp transition from predominantly red to much bluer colors at approximately $z = 0.65$. The bluest quasars have z around 1, while the more distant ones at $z > 1.4$ do not show much variation in color.

Fig. 5, left panel, displays the median parallax of 2466 ICRF3 objects (with carefully cleaned and vetted optical counterparts) for bins of sorted BP–RP color of equal size (246). We find a complex and unexpected behavior of the parallax zero-point error with the object’s color. Starting below $-40 \mu\text{as}$ for the bluest quasars, the parallax increases to zero at $\text{BP} - \text{RP} \approx 0.6$, but it suddenly drops back to below $-40 \mu\text{as}$ at $\text{BP} - \text{RP} \approx 0.7$. This sharp transition hints at an instrumental effect. The average zero-point value for our sample results from this strong dependence and the distribution of colors, but the latter is sample-specific, so other studies can indeed arrive at different estimates in the range between 0 and $-50 \mu\text{as}$. Apparently, there is a calibration issue comparable in magnitude to the zero-point bias itself.

5. A cosmological factor in the radio-optical offsets?

Both Gaia DR1 and DR2 data show a large excess of position differences outside of the expected dispersion due to purely astrometric errors. Based on the Gaia DR1 astrometric data, Makarov et al. (2017) estimated that more than 4% of ICRF2 sources with optical

³http://docs.astropy.org/en/stable/api/astropy.stats.biweight_location.html.

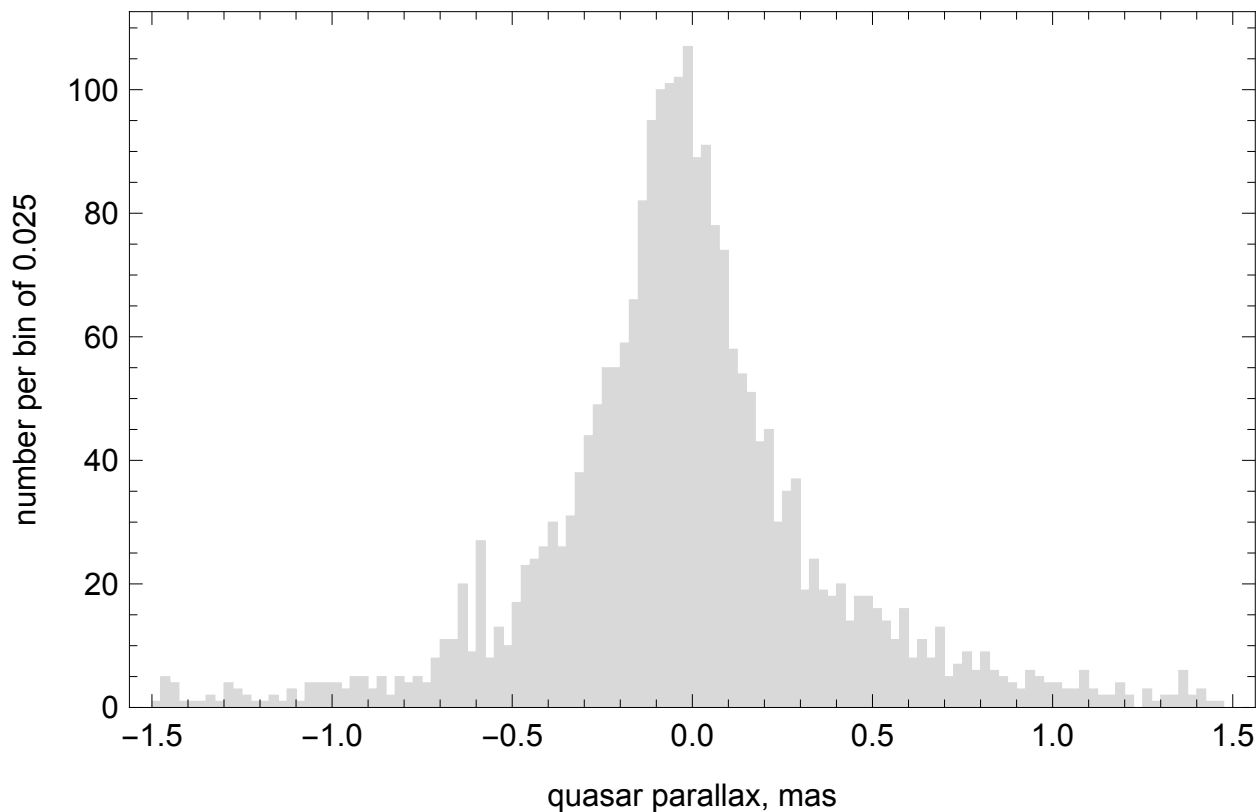


Fig. 4.— Histogram of Gaia DR2 parallaxes for 2465 counterparts of ICRF3 radio-loud quasars.

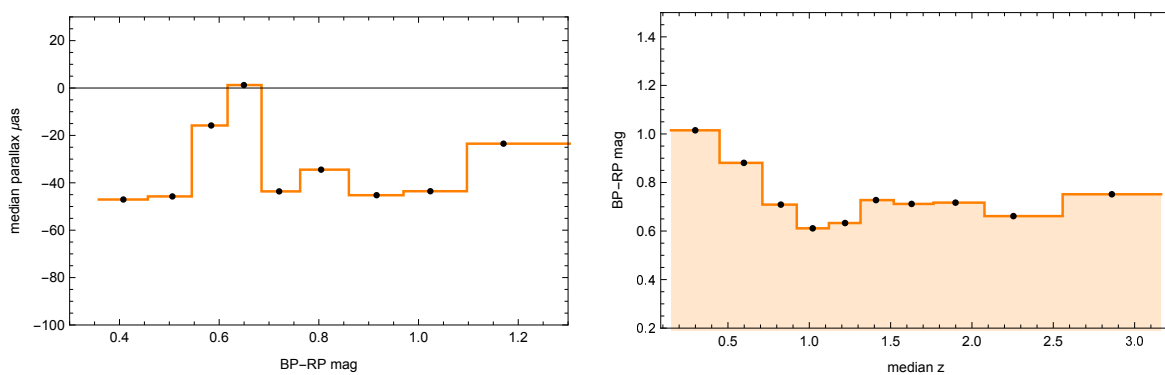


Fig. 5.— Left: binned median parallax of ICRF3 sources versus color BP–RP in Gaia DR2. The bin size is 246 objects. The estimated error of the mean parallax for each bin is $16 \mu\text{as}$. Right: binned median color BP–RP in Gaia DR2 versus redshift z . The bin size is 205 objects.

counterparts passing all available quality filters (single, point-like, unperturbed) have position differences outside of the statistical expectancy. It was suggested that the AGNs in these distant objects are physically “dislodged”, i.e., they are not located in the optical centers of the host galaxies. This hypothesis will be testable when high-precision epoch astrometry from Gaia becomes available in the future releases. Some of the AGNs are highly variable in the optical, while the host galaxy is constant. The photocenter of a variable source blended with an offset constant source displays a coherent Variability-Induced Motion (VIM) effect (e.g., Makarov & Goldin 2016), where the astrometric displacement is correlated with the light curve. An alternative explanation was proposed by Petrov & Kovalev (2017) and citetpla, where the observed displacement is caused by milliarcsecond-scale jets luminous enough in the radio to cause a photocenter shift. With different parts of a relativistic jet being responsible for the most compact source of emission detected by the VLBI, the optical photocenter can be shifted from a relatively larger contribution of the accretion disk.

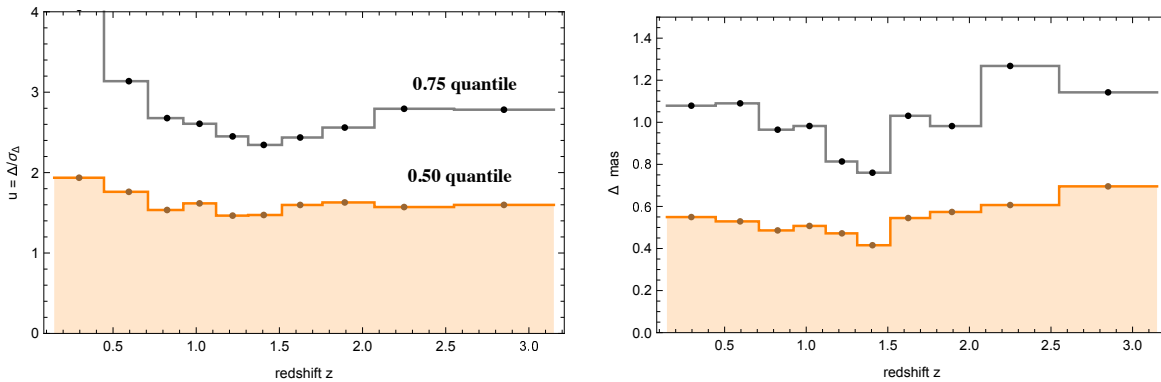


Fig. 6.— Median (0.50 quantile) and 0.75 quantile of relative offsets Δ/σ_{Δ} (left) and absolute offsets Δ in mas (right) versus redshift z for cross-matched ICRF3 sources in Gaia DR2. The estimated uncertainties of the medians for each bin are 0.063 for u and 0.030 mas for Δ .

Both these interpretations can be indirectly tested using the observed relation between the offsets and cosmological redshifts. The OCARS catalog conveniently includes the redshifts for most of the objects collected from the literature. We are using the redshifts only for large-number statistical estimation. The starting assumption is that the observed angular displacement depends on the distance to a given AGN, if the typical physical displacement (or jet) has a certain characteristic size in the object’s comoving frame. More distant objects would be statistically less displaced in the angular measure, but the spacetime is not flat, and a more complicated relation emerges, depending on the cosmological model of the universe. The relevant parameter is the “angular diameter distance”, which is a nonlinear function of redshift. Most of the “standard” models predict that this distance rapidly rises with z at small z , peaks at roughly $z = 2$, and becomes either flat or is slowly declining

at higher redshifts. This should give a concave curve on a “offset versus redshift” diagram. To test this prediction, we performed the following calculation. The vetted quasars with available redshifts (counting 2074 objects) were sorted by z and divided into 10 equal bins of 207 objects each. Each subsample covers a certain range of redshifts. The 0.50 (median) and 0.75 quantiles of the normalized offset u were computed for each bin of redshifts. The results are shown in Fig. 6. Both quantile offsets become smaller with increasing z at small values, as expected, but the decline is rather slow. The offsets reach a minimum at $z \simeq 1.5$, followed by a small step-up. This increase in offsets is more visible in absolute position differences ($\Delta = \sqrt{d_1^2 + d_2^2}$), right plot, than in normalized offsets u , left plot. The jump of median Δ at 1.5 is from 0.42 to 0.58 mas. For $z > 1.6$, the dependence becomes rather flat for u and steadily increasing for Δ . These differences are possibly caused by the distribution of G magnitudes, which become fainter with increasing z , making the formal errors of Gaia rapidly grow.

This relation may seem at odds with the predictions of standard models. Of course, our starting assumption that the physical size of displacement is independent of z may be incorrect. But the experiment indicates a nonmonotonic factor missing in the model. It is possible that the measured offsets (or their formal errors) are subject to an unidentified instrumental error in the Gaia data. This error may be magnitude-dependent. The quasars become generally fainter with increasing z at redshifts greater than 1.2, but the dependence is fairly smooth and no feature is visible around $z = 1.5$. An instrumental systematic error can also be color-dependent. Lindegren et al. (2018) describe the limitations of the color-dependent calibration in the Gaia DR2. A similar analysis of the median color BP–RP versus redshift is shown in Fig. 5, right panel. It reveals that the nearest radio-loud quasars are red, but the color becomes bluer by almost 0.4 mag at $z \simeq 1$, where a global minimum is observed. The color becomes slightly redder again by $z \simeq 1.5$, after which it becomes flat or slightly declining. This complex behavior of color versus z may look unexpected, but photometric analysis of completely independent Pan-STARRS data (C.T. Berghea et al. 2019, in preparation) shows a similar pattern in the $r_{\text{PS1}} - z_{\text{PS1}}$ color. The rise at $z \simeq 1.4$ may be caused by the relatively bright emission line Mg II $\lambda 2798$, which shifts from the BP to the RP spectral window (roughly corresponding to the Sloan Digital Sky Survey – SDSS– i band) at this redshift. Similar small reddening in median colors have been noted in other photometric investigations (Croom et al. 2004; Meusinger et al. 2011). For the broad G band, where Gaia astrometric measurements are taken, the C IV emission line may be of greater importance, emerging within the band at $z \gtrsim 1.6$. Fig. 7 displays the spectrum of IERS 1319 + 220, which is one of the quasars that pass all the quality criteria described in this paper, but are not included in the precious set on account of elevated offsets ($u > 3$). At $z = 1.685$, the dominating C IV emission line is well within the G -band at its cutoff

around 400 nm. If the source of emission in this line is physically displaced from the source of the radio emission, a measurable offset in positions occurs. The cross-over of the C IV line into the Gaia astrometric band happens at $z = 1.6$, as can be seen from comparison of SDSS spectra for IERS 1235 + 196 at $z = 1.533$ and 1232 + 366 at $z = 1.598$. Other emission line cross-overs of note are for the lines C III at $z = 1.1$ and Ly_α at $z = 2.3$. For example, the spectrum of the ICRF3 QSO 1337 + 637 ($z = 2.56$) is dominated by a Ly_α line at approximately 425 nm. There are also strong C IV and C III lines present within the G band. This object has a large Gaia–ICRF3 offset, which left it out of the precious set. We do not find signs of astrometric perturbation associated with the emergence of this line in Fig. 6, except for a possible bump in the 0.75 quantile of absolute offsets (right plot).

6. Conclusions

Our previous analysis based on Gaia DR1 and ICRF2 data (Makarov et al. 2017) determined that the core distribution of Gaia–VLBI position offsets was consistent with the expected PDF, but a significant fraction of the matches had large differences in positions that could not be explained by the estimated random or systematic errors. The tremendous improvement of astrometric precision achieved in Gaia DR2 for faint objects (Lindgren et al. 2018), where its level is already close to the expected 5 yr mission performance (Brown and Gaia Collaboration 2018), reveals a greater rate of radio-loud objects with significant offsets in optical positions. Even after a rigorous cleaning of the sample with astrometric quality filters and image-based vetting, we arrived at a sample that includes 20% of objects with normalized differences above 3, where the expected rate of outliers is 1%. This implies that a significant fraction of RORF objects, which can be accurately measured both by VLBI and Gaia, are perturbed by a “cosmic error” (called DARN in Zacharias & Zacharias (2014)). The origin of this perturbation may be in the nonstellar morphology of the sources. The angular resolution of Gaia is still much lower than that of VLBI, and the galactic substrates, blended cores of optical emission, gravitational lenses, and jets, can cause the optical photocenters to shift from the more constrained radio positions. A fraction of RORF objects can also be physically displaced with respect to their host galaxy centers (Skipper & Browne 2018). This may be the main explanation for relatively nearby AGNs ($z \lesssim 1$), which are typically redder with a significant contribution of their host galaxies in the flux. Additionally, the Gaia low-level data pipeline has not been tuned to centroid complex or extended sources. Petrov et al. (2019) used a much larger compilation of VLBI sources (but with less precise positions) for a similar study. They estimated the rate of statistically significant offsets at 9%, but this estimate was obtained after inflating both the VLBI and Gaia formal uncertainties. It is likely that the ICRF3 positions are more pre-

RA=200.54754, DEC=21.80340, MJD=54508, Plate=2652, Fiber=475

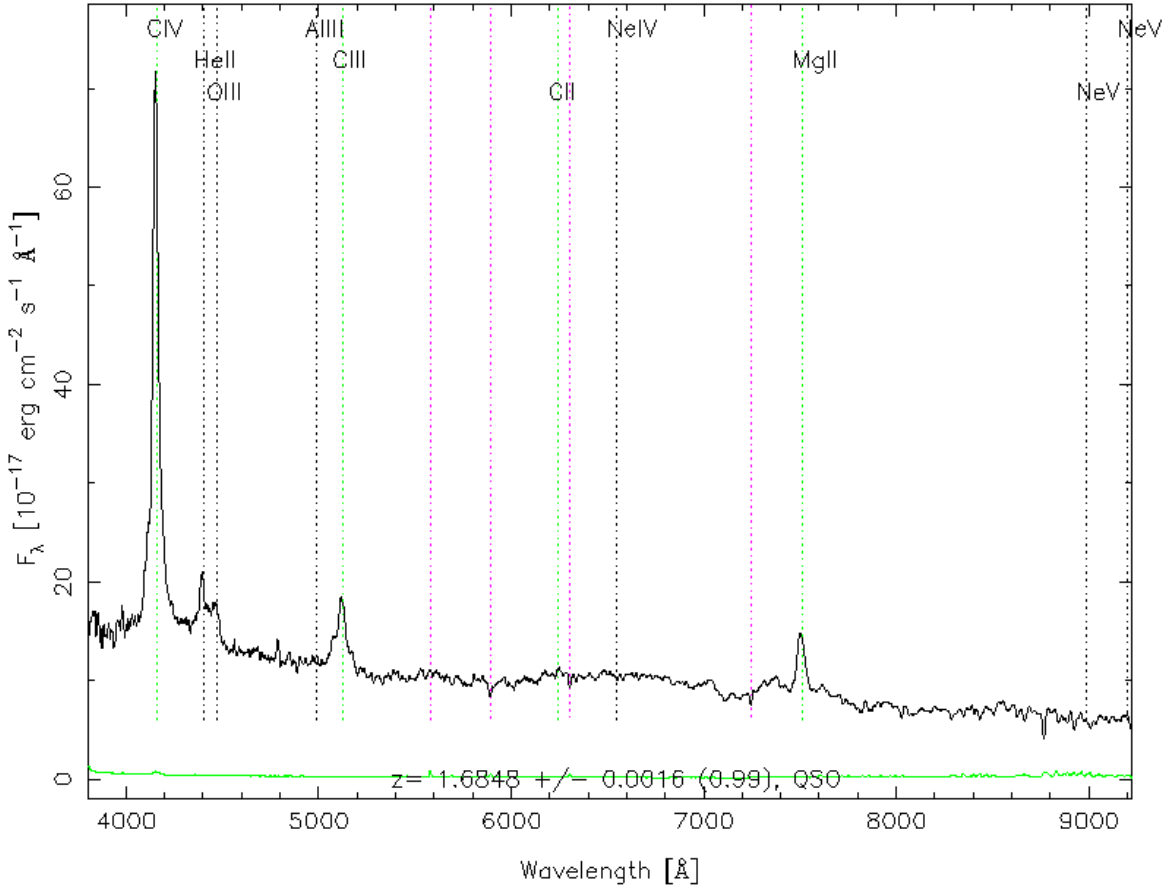


Fig. 7.— SDSS7 spectrum of the ICRF3 QSO 1319 + 220 at $z = 1.685$. The emission spectrum is dominated by the C IV line, which appears at the blue edge of the G -band sensitivity window for $z > 1.6$.

cise than the larger collections of VLBI positions, which allows us to avoid modifications to estimated coordinate variances in this analysis. A preliminary solution for ICRF3 positions analyzed by Frouard et al. (2018) showed a closer agreement with Gaia DR1 than ICRF2 positions.

Once the reality of this perturbation is established, the strategy of using RORF needs to be changed. They are still indispensable as the main method to tie the two reference frames. Those quasars that have large position offsets, as interesting and enigmatic they may be from the astrophysical point of view, are practically useless as RORF objects. Their inclusion would do more harm than good to the effort of bringing together the reference frames. Petrov et al. (2019) also caution against using RORF sources as absolute reference for proper motions, because photometric variability of the central emission-line regions may cause the optical photocenter to move mimicking astrometric angular motion. In this paper, we determined and published a set of 2118 radio-optical quasars that are not perturbed too strongly, and, therefore, can still be used to determine the orientation of the Gaia coordinate system in space.

The improved precision of the optical data also allows us to look at the possible cosmological relation of the offsets. The median position offset (and its higher quantiles), both in absolute and relative measure, shows an unexpected feature at redshift $z \approx 1.5$, where the generally concave and smooth dependence appears to be broken. We suggest that this peculiarity may be related to the emergence of the C IV emission line at the blue edge of the G -band spectral sensitivity window. We examined multiple optical spectra of the 524 sources that pass the astrometric quality criteria but still have large optical-radio position offsets. There seems to be two broad categories of spectra present, namely, relatively nearby objects with weak or invisible emission lines (e.g., IVS 1204+057), or QSO with powerful redshifted Mg II ($z > 0.45$), C III ($z > 1.1$), C IV ($z > 1.55$), or even Ly $_{\alpha}$ ($z > 2.5$) located closer to the blue end of the astrometric band. The former category may comprise BL Lac-type objects, despite our conscious effort to remove them early in the analysis, which are known to have larger astrometric offsets from previous publications. The latter category indicates that the compact sources of radio-emission that form VLBI sources may be displaced from the broad-line. To confirm or disprove this behavior, more accurate and internally consistent astrometric observations of RORF objects are needed, especially at declinations less than -30° , where ICRF3 is conspicuously sparse. Future Gaia data releases may help to clarify the matter, although the advance in astrometry is not expected to be drastic for these mostly faint objects. High-resolution imaging has proven helpful for this analysis, and we have made a first step with collecting a library of best-quality optical images of these radio-loud sources. A more consistent effort with space-borne telescopes may be justified in the future, given the importance and relative scarcity of RORF objects. Finally, a systematic spectroscopic and

photometric investigation of ICRF3 sources is in order, especially in the sky areas outside of the SDSS footprint.

If the reason for the commonly present increased perturbation of radio-loud quasars is based in the astrometric properties of Gaia, it should also be reflected in the observed parallaxes and proper motions. These data have been used for verification and validation of Gaia DR2 data (?). We do not find any significant correlation between the error-normalized position offsets and parallaxes within our precious set of RORF objects. This supports the notion that the large offsets are intrinsic. The negative bias of quasar parallaxes is quite prominent for this sample, and we find it to be color-dependent in a complex way, hinting at a chromatic calibration issue in Gaia.

Low-redshift sources do have distinctly greater radio-optical offsets. This can be explained in different ways, including a relatively larger contribution of extended galaxy images, but the most straightforward interpretation assumes that a certain physical separation between the most luminous components yields a smaller angular resolution in the observer’s frame at greater distances. A large fraction of radio-loud quasars display rather extreme variability on the time scales of a month and less, both in the optical and the X-band (Barvainis et al. 2005). Comparative analysis of simultaneous photometric observations in the optical and radio passbands could perhaps reveal if the same components of AGN machines are observed.

7. Acknowledgments

This work has made use of data from the European Space Agency (ESA) mission *Gaia* (<http://www.cosmos.esa.int/gaia>), processed by the *Gaia* Data Processing and Analysis Consortium (DPAC, <http://www.cosmos.esa.int/web/gaia/dpac/consortium>). Funding for the DPAC has been provided by national institutions, in particular the institutions participating in the *Gaia* Multilateral Agreement. The Pan-STARRS1 Surveys (PS1) have been made possible through contributions of the Institute for Astronomy, the University of Hawaii, the Pan-STARRS Project Office, the Max-Planck Society and its participating institutes, the Max Planck Institute for Astronomy, Heidelberg and the Max Planck Institute for Extraterrestrial Physics, Garching, The Johns Hopkins University, Durham University, the University of Edinburgh, Queen’s University Belfast, the Harvard-Smithsonian Center for Astrophysics, the Las Cumbres Observatory Global Telescope Network Incorporated, the National Central University of Taiwan, the Space Telescope Science Institute, the National Aeronautics and Space Administration under grant No. NNX08AR22G issued through the Planetary Science Division of the NASA Science Mission Directorate, the National Science Foundation under

grant No. AST-1238877, the University of Maryland, and Eötvös Loránd University (ELTE) and the Los Alamos National Laboratory. This project used public archival data from the Dark Energy Survey (DES). Funding for the DES Projects has been provided by the U.S. Department of Energy, the U.S. National Science Foundation, the Ministry of Science and Education of Spain, the Science and Technology Facilities Council of the United Kingdom, the Higher Education Funding Council for England, the National Center for Supercomputing Applications at the University of Illinois at Urbana-Champaign, the Kavli Institute of Cosmological Physics at the University of Chicago, the Center for Cosmology and Astro-Particle Physics at the Ohio State University, the Mitchell Institute for Fundamental Physics and Astronomy at Texas A&M University, Financiadora de Estudos e Projetos, Fundação Carlos Chagas Filho de Amparo à Pesquisa do Estado do Rio de Janeiro, Conselho Nacional de Desenvolvimento Científico e Tecnológico and the Ministério da Ciência, Tecnologia e Inovação, the Deutsche Forschungsgemeinschaft, and the Collaborating Institutions in the Dark Energy Survey. The Collaborating Institutions are Argonne National Laboratory, the University of California at Santa Cruz, the University of Cambridge, Centro de Investigaciones Energéticas, Medioambientales y Tecnológicas-Madrid, the University of Chicago, University College London, the DES-Brazil Consortium, the University of Edinburgh, the Eidgenössische Technische Hochschule (ETH) Zürich, Fermi National Accelerator Laboratory, the University of Illinois at Urbana-Champaign, the Institut de Ciències de l’Espai (IEEC/CSIC), the Institut de Física d’Altes Energies, Lawrence Berkeley National Laboratory, the Ludwig-Maximilians Universität München and the associated Excellence Cluster Universe, the University of Michigan, the National Optical Astronomy Observatory, the University of Nottingham, The Ohio State University, the OzDES Membership Consortium, the University of Pennsylvania, the University of Portsmouth, SLAC National Accelerator Laboratory, Stanford University, the University of Sussex, and Texas A&M University. This paper makes use of data based in part on observations at Cerro Tololo Inter-American Observatory, National Optical Astronomy Observatory, which is operated by the Association of Universities for Research in Astronomy (AURA) under a cooperative agreement with the National Science Foundation. This research uses services or data provided by the NOAO Data Lab. NOAO is operated by the Association of Universities for Research in Astronomy (AURA), Inc. under a cooperative agreement with the National Science Foundation.

REFERENCES

- Arenou, F., Luri, X., Babisiaux, C., et al. 2018, *A&A*, 616, A17
- Barvainis, R., Lehar, J., Birkinshaw, M., et al. 2005, *ApJ*, 618, 108

- Berghea, C.T., Makarov, V.V., Frouard, J., et al. 2016, *AJ*, 152, 53
- Brown, A.G.A., and Gaia Collaboration. 2018, *A&A*, 616, A1
- Chambers, K. C., Magnier, E. A., Metcalfe, N., et al. 2016, ArXiv e-prints [arXiv:1612.05560]
- Croom, S.M., Smith, R.J., Boyle, B.J., et al. 2004, *MNRAS*, 349, 1397
- Fabrizius, C., Bastian, U., Portell, J., et al. 2016, *A&A*, 595, 3
- Fey, A., Gordon, D., Jacobs, C.S., et al. 2015, *AJ*, 150, 58.
- Frouard, J., Johnson, M., Fey, A., et al. 2018, *AJ*, 155, 229.
- Hamilton, T.S., Casertano, S., Turnshek, D.A. 2008, *ApJ*, 678, 22.
- Kopeikin, S.M., Makarov, V.V., *AJ*, 131, 1471
- Lindgren, L., Hernández, J., Bombrun, A., et al. 2018, *A&A*, 616, A2
- Magnier, E.A., , Schlafly, E., Finkbeiner, D., et al. 2013, *ApJS*, 205, 20
- Makarov, V.V., Berghea, C., Boboltz, D., et al. 2012, *MmSAI*, 83, 952
- Makarov, V.V., Frouard, J., Berghea, C., et al. 2017, *ApJ*, 835, L30
- Makarov, V.V., Goldin, A. 2016, *ApJS*, 224, 19
- Malkin, Z.M. 2016, *Astronomy Reports*, 60, 996
- Malkin, Z. 2013, *Izvestiia Glavnoi Rossiiskoi Astronomicheskoi Observatorii Pulkovo*, 220, 507
- Meusinger, H., Hinze, A., de Hoon, A. 2011, *A&A*, 525, A37
- Mignard, F., Klioner, S., Lindgren, L., et al. 2016, *A&A*, 595, 5
- Morganson, E., Gruendl, R.A., Menanteau, F., et al. 2018, *PASP*, 130, 450
- Orosz, G., Frey, S. 2013, *A&A*, 553, 13
- Petrov, L., Kovalev, Y.Y. 2017, *MNRAS*, 467, L71
- Petrov, L., Kovalev, Y.Y. 2017, *MNRAS*, 471, 377
- Petrov, L., Kovalev, Y.Y., Plavin, A.V. 2018, *MNRAS*, 482, 3023

- Plavin, A.V., Kovalev, Y.Y. Petrov, L. 2018, ArXiv e-prints [arXiv:1808.05115]
- Prusti, T., de Bruijne, J.H.J., Brown, A.G.A., et al. 2016, *A&A*, 595, 1
- Schlafly, E.F., Finkbeiner, D.P., Jurić, M., et al. 2012, *ApJ*, 756, 158
- Secrest, N., Dudik, R.P., Dorland, B.N., et al. 2015, *ApJS*, 221, 12
- Skipper, C.J., Browne, I.W.A. 2018, *MNRAS*, 475, 5179
- Titov, O., & Malkin, Z. 2009, *A&A*, 506, 1477
- Tonry, J.L, Stubbs, C.W., Lykke, K.R., et al. 2012, *ApJ*, 750, 99
- Zacharias, N., & Zacharias, M.I. 2014, *AJ*, 147, 95